Research

Application of frequency selection and geoelectrical sounding methods for mapping of leachate's pathways in an active dumpsite

Theophilus Aanuoluwa Adagunodo[1] · Ayobami Ismaila Ojoawo[2] · Nicholas Oliseloke Anie[3] · Praise Oforitsenere Edukugho[1]

Abstract

Contamination of surrounding environments is one of the threats to the proper maintenance of municipal waste sites in developing nations. This study integrates natural electromagnetic (EM) field and geoelectrical sounding methods to assess the leachate's pathways in the near-surface layers and groundwater system in and around an active dumpsite. Five natural EM traverses were obtained in varying orientations using PQWT-TC 150 model. Fifteen vertical electrical sounding (VES) data points were randomly occupied using SAS 4000 ABEM resistivity meter. The two techniques revealed some intercalations of conductive and resistive media in the study area. The conductive media are composed of mixtures of leachates into clay and groundwater units, thereby creating zones of very low electrical potential differences from the surface to a depth beyond 30 m. A zone of leachate-aquifer's interphase exists between the third layer and the fourth layer. The directions of the fluid flow are in the S–N and SE–NW trends, which could be linked to the fault towards the northwestern part of the study area. The fluid dynamics, however, justified the reason for the thick conductive materials being mapped at the northwestern and northern parts of the study area.

Article Highlights

- An attempt was made to use the frequency selection method (FSM) in environmental study.
- There is a synergy between the FSM results and the geoelectrical sounding results.
- The depths of leachate's mixing into the aquiferous units varied from 4.0 to 30.0 m.

1 Introduction

The most common waste disposal channel in Africa and Asia is the disposal of waste materials in open solid waste sites [1]. This kind of practice has become a threat to the lives of people living within the axis of the waste site(s) [2]. Examples of the resulting challenges to the biotic system within the waste sites include soil degradation, air

✉ Theophilus Aanuoluwa Adagunodo, taadagunodo@yahoo.com; taadagunodo@gmail.com | [1]Department of Physics, Covenant University, Ota, Ogun State, Nigeria. [2]Department of Physics, University of Ibadan, Ibadan, Oyo State, Nigeria. [3]Physics Unit, Federal School of Surveying, Oyo, Nigeria.

pollution and (surface and ground) water pollution [3]. Leachates could emanate from residential or industrial waste environments. It contains a high concentration of suspended or soluble materials. The waste material's pathways into the (shallow or deep) aquifer could be through an increase in the water table (during the rainy season), the absence of confining layers above the aquiferous medium and faulting systems of the parent rocks [4]. The major sources of pollution are point-source and nonpoint-source (or area) pollution. The point-source pollution could arise from landfills, accidental spills, industrial waste sites and leakages of underground tanks, while the nonpoint-source pollution could eventuate through the use of herbicides, pesticides and fertilizers in an agricultural domain. The two sources of pollution are deleterious to man when pollutants find their way into the aquifer. Thus, it is imperative to map the leachate pathways in the subsurface to ensure that the groundwater (to be used for domestic and industrial purposes) is not exploited from the polluted aquifer.

There are numbers of developed techniques for the characterization and mapping of leachate pathways. Some of these techniques had produced insufficient subsurface imaging, leading to an indecisive remedial approach. Geophysical techniques had proved to bridge the gap, by producing well-established subsurface information [5]. In this study, the 2D electromagnetic (EM) technique (which is based on the frequency selection method (FSM) of the Earth's natural EM field) and electrical resistivity (ER) method (which adopts the Schlumberger configuration) were integrated to map the leachate's pathways from an active dumpsite in Amuloko, Ibadan, southwestern Nigeria.

The very low frequency-EM (VLF-EM) and the ER techniques have been used in the time past for leachate's mapping. The VLF-EM, which operates within 10–30 kHz frequency, is used to map the presence of conductive bodies at the shallow near-surface (< 30 m) [6]. The most adopted ER configurations in the past are Wenner and Schlumberger. The Wenner array is used to map the lateral variations, while the Schlumberger array images the vertical variations in the near-surface media [7]. Engaging in multiple Wenner array profilings for electrical resistivity imaging campaign in the subsurface mapping of contaminant's flow had been reported to be tedious [8] in comparison to the EM survey using the natural electric field [9]. The EM survey (using the natural electric field) is faster and penetrates deeper than other geophysical methods for near-surface exploration [10].

The FSM is generally assigned to various methods being proposed by Chinese scholars in the early 1980s. Consecutively, such as the FSM of telluric current, natural low-frequency E-field method, audio geoelectric/earth potential (or stray current) method, E-pulse method of natural field, sound frequency geoelectric/earth field method, natural alternating field method, interference E-field method, geoelectric FSM, underground magnetic fluid detection method, audio frequency telluric electricity method, and so on. The FSM is a passive source EM sounding exploration method. It operates on the variation of electrical conductivity between subsurface rocks, using magnetotelluric field as the source of the working field. The FSM is an enhancement of audio frequency telluric electricity method. The field operations of FSM and audio magnetotelluric method (AMT) are the same; nevertheless, FSM only measures the horizontal components of the E-field at various frequencies, but does not measure the H-field of EM signals in the subsurface [10, 11]. As recently posited by Yang et al. [11], the anomalous signatures of the FSM are total reflections of the static shift in the magnetotelluric sounding.

Most of the FSM geophysical machines (such as PQWT and ADMT series) measuring the electric potential difference (in Volts) are cheap, easy and fast to use for geophysical survey, penetrates deeper, overcome surrounding or terrain restrictions easily, associated with uncomplicated operations and not heavy to carry, unlike the conventional geophysics machines [12]. Currently, the frequencies of the FSM ≈ varies from 0.01 to 5 kHz, with the potential electrode spacing (MN) for profiling at 10 or 20 m. FSM machines are receiving attention in today's geophysical studies, especially in some developing countries. Though some geoscientists still doubt its acceptability as part of the available and cost-effective equipment for geophysical campaigns, this opinion is borne out of the fact that the FSM is not among the common geophysical methods. Some rejected its applicability in exploration geophysics because they could not relate its mode of operations with the available scientific principles [10–13]. Also, the absence of the total measured unit(s) on the display screen (which requires the immediate attention of the manufacturer) has made some geoscientists condemn its usefulness in geophysical studies. To increase the scope of its applications in geophysics, the PQWT is integrated with the ER method for environmental study over a crystalline basement complex.

The ER adopting vertical electrical sounding (VES) configuration has shown its effectiveness in groundwater exploration, geotechnical studies and environmental studies. The global adoption of VES for mapping near-surface structures had been linked to its simplicity, equipment's ruggedness and easy interpretation of the acquired data [13, 14]. In ER method, an active geophysical method, the inferred geological sequences are functions of the subsurface media, porosity as well as the formation's water content [14, 15]. Soil and rocks are poor conductors. The

penetrated subsurface media (soil and rocks) by leachates could retain appreciable quantities of dissolved ions that are capable of increasing the conductivity of such media. Generally, data obtained from electrical methods are expected to possess moderate resistivity signatures for media filled with fresh water, while media filled with dissolved ions as a result of leachate's infiltration are characterized by very low resistivity signatures. The aim of this study is to map the leachate's pathways into the aquifer system within an active dumpsite in Ibadan, southwestern Nigeria. The objectives of this study are to determine the: (i) vertical depths at which the leachates had infiltrated into the aquifer; (ii) number of geo-electrical sequences and inferred lithologic units within the mapped zone; (iii) number of aquifers and the groundwater potential of the most viable aquifer; and (iv) leachate's migration paths and directions of fluid flow in the study area. This study seeks to achieve agendas 3, 6 and 11 of the Sustainable Development Goal (SDG), which aims at ensuring that all lives (at all ages) are healthy; to guarantee the sustainable sanitation for all; and to make sure that cities and human settlements are safe and sustainable [16].

2 Descriptions and geological mapping of the study site

Ibadan is one of the megacities in Nigeria. It is situated on the southwestern axis of Nigeria with a population of ≈ 3 million people [17]. Its coordinates are bounded by latitude 7° 20′ to 7° 40′ north and longitude 3° 35′ to 4° 10′ east. Ibadan lies within a humid and sub-humid tropical climate. The rainy season varies from March to October, while the dry season spans from November to February. The average rainfall of about 1230 mm is recorded annually in Ibadan, with the temperature varying from 21 to 35 °C [17].

Ibadan falls on the crystalline basement rocks of southwest Nigeria (Fig. 1a), which is of Precambrian age. The basement rocks are chiefly composed of metamorphic and crystalline rocks [18]. Major intrusions within the metamorphic rocks of Ibadan are granites and porphyries. Weathered regoliths are the most appearing rocks in Ibadan. Three-quarter of the weathered rocks are of banded gneiss, while quartzites and augen gneisses share the remaining one-quarter of the entire geological settings in Ibadan [19]. As revealed in Fig. 1b, rocks such as undifferentiated gneiss complex, granite gneiss, amphibolites, pegmatite, migmatite gneiss, quartzite quart schist, quartz vein and banded gneiss are found in Ibadan and its environs.

The solid wastes being generated daily in Ibadan have increased rapidly to about 1,618,293 kg [19]. The four

approved locations by the state management authority for the final disposal of these wastes in Ibadan are Lapite, Aja-kanga, Awotan and Amuloko. These four locations could only cater for about one-quarter of the total waste being generated in Ibadan on a daily basis. The study area is situated in the southeastern part of Ibadan (Fig. 1b). A river flowing in the W–E direction is present at the northern part of the dumpsite (about 7 m away from the dump) (Fig. 1b). The age of the dumpsite is ≈ 3 decades. It is situated in a lowland environment. The topography towards the northwestern part is a valley-like terrain. An overview of the western side is revealed in Fig. 1c. The pronounced rock formation in the study area is the granite gneiss, which is an assemblage of minerals such as quartzes and feldspars.

The hydrogeological order that governs the accumulation and flow of groundwater in Amuloko is of the crystalline basement rocks. At the unaltered state of the basement rocks, it is distinguished by low groundwater yield, as a result of low pore spaces and poor interconnectivities. The groundwater yield increases as soon as the bedrock becomes weathered and fractured, thereby resulting in the development of secondary pore spaces and great interconnectivity. The newly formed porosity and permeability of the weathered or fractured bedrock control the transmissivity of the aquifer system in crystalline bedrock [17]. Some fault networks, which aid the permeability of aquiferous units in the basement terrain, exist in Ibadan [20]. A range of 1 to 6 m was recorded as the water table's depths in the study area.

3 Materials and methods

The materials employed in this study include a compass, global positioning system, measuring tapes, hammers, connecting cables and reels, an EM meter using PQWT equipment, ER meter using SAS 4000 ABEM series equipment and other geophysical kits for geophysical survey. The procedure adopted in this present study involves geophysical data acquisition and detailed data analyses. Before the data acquisition, a reconnaissance survey and literature search for a detailed understanding of the local geology of the study location were done. Physical features around the dumpsite were also taken into consideration before the choice of methods adopted in the present study.

Five EM traverses were obtained (Fig. 1d) using PQWT-TC 150 model. A PQWT-TC 150 is capable to probe up to 150 m depth. The range of the sounded points per traverse varied from 9 points (at traverse 1) to 19 points (at traverse 5). An inter-data point interval of 2 m was used for the acquired EM data in this study. A distance of 10 m was used between the two probes (MN) [9]. The PQWT is an automated
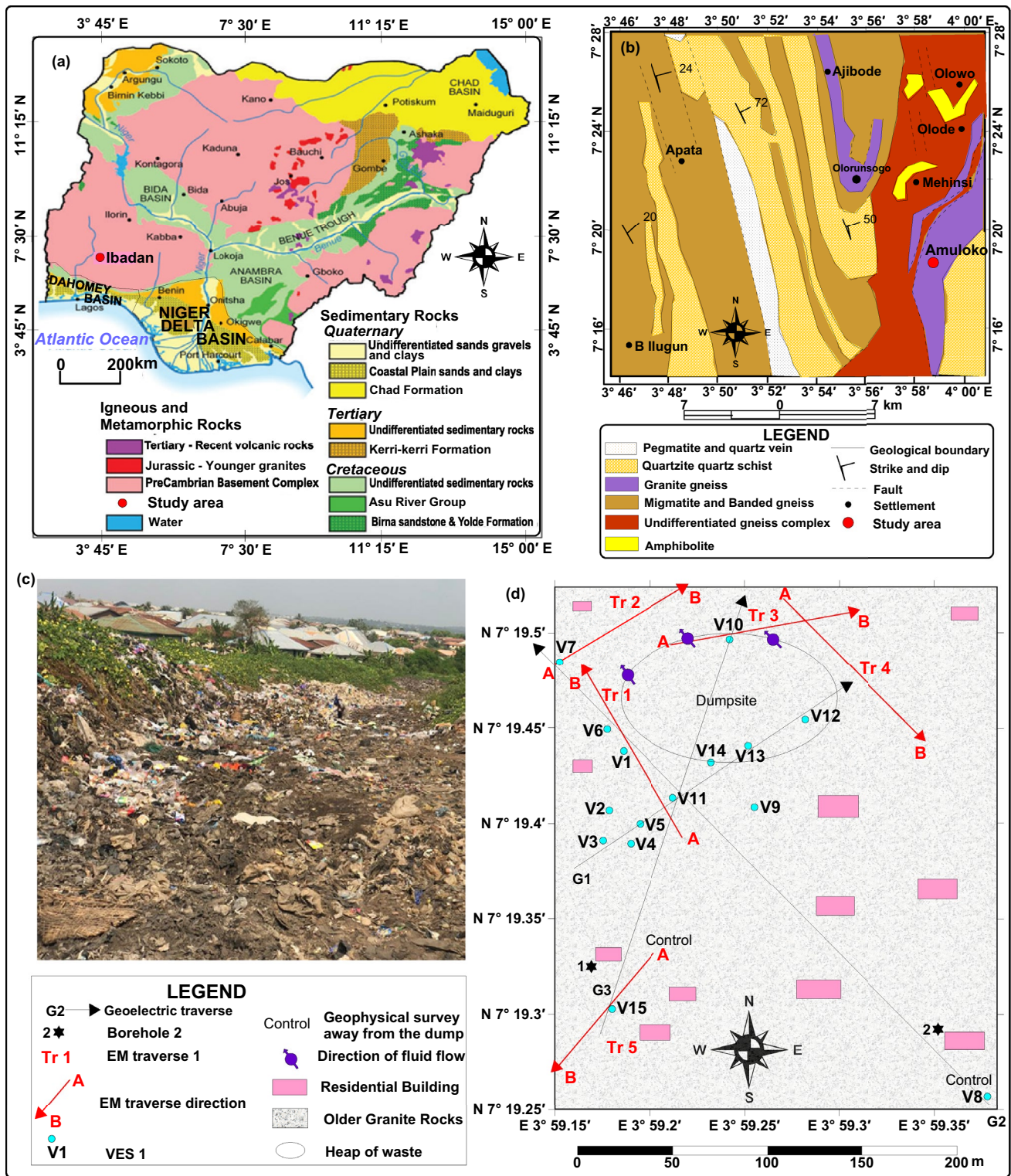
Fig. 1 **a** Geological map of Nigeria (reproduced from [18]), **b** Geological map of Ibadan showing the study location (reproduced from [17]), **c** Overview of the western part of Amuloko dumpsite, **d** Base map of the dumpsite

geophysical prospecting equipment with high sensitivity. It uses an EM field of the Earth as the source, which measures the potential difference between two terminals on the

Earth's surface being generated by the natural electric current in the near-surface [13]. The subsurface natural electric current is produced through electrochemical processes

among various conductive minerals being in contact with one another, and the fluid contents in porous media within the subsurface. The electric field (E-field) component of the Earth's EM field at various frequencies are measured in millivolt. The natural E-field is used to determine the resistivity contrast of various geologic bodies with respect to the lithological units of the near-surface. When the variations of the E-field generated by the natural EM field at various frequencies are observed, the change in electrical conductivity of the ore or rock bodies at different subsurface depths can be analyzed to infer the positions of the anomalies [12]. The magnetotelluric field is more or less considered as a plane EM wave incident perpendicular to the Crust.

When the EM waves are sent to the subsurface, where the electrical conductivity $\sigma \neq 0$, the free charge cannot be clamped at a point, so that the magnetotelluric field's propagation obeys the Maxwell's equations (as shown in Eqs. (1) and (2)).

$$\nabla \times E = iw\mu H \tag{1}$$

$$\nabla \times H = (\sigma - iw\varepsilon)E \tag{2}$$

where E, H, w, μ, ε and σ are E-field (V.m^{-1}), H-field (A.m^{-1}), angular frequency (rad.s^{-1}) (with $w = 2\pi f$), magnetic permeability (H.m^{-1}), dielectric permittivity (F.m^{-1}) and electrical conductivity (mS.m^{-1}) (with $\rho = 1/\sigma$ (Ω.m), respectively. The imaginary unit, $i = \sqrt{-1}$, $i^2 = -1$, and f is the frequency (Hz).

As the EM field propagrates vertically downward (along the z axis) as plane waves in a three-dimensional system, the Maxwell's equations are expanded, and two independent polarization modes (that is, transverse electric (TE) and transverse magnetic (TM) fields) are obtained [11]. Since the FSM only determines the E-field along the horizontal component of the survey line (E$_y$), the E$_y$ can be calculated by Eq. (3).

$$E_y = \frac{1}{\sigma - iw\varepsilon} \frac{\partial H_x}{\partial z} \tag{3}$$

where H$_x$ satisfies the partial differential equation in Eq. (4):

$$\frac{\partial}{\partial y}\left(\frac{1}{\sigma - iw\varepsilon}\frac{\partial H_x}{\partial y}\right) + \frac{\partial}{\partial z}\left(\frac{1}{\sigma - iw\varepsilon}\frac{\partial H_x}{\partial z}\right) + iw\mu H_x = 0 \tag{4}$$

Therefore, the apparent resistivity $\left(\rho_a^{TM}\right)$, the impedance $\left(Z^{TM}\right)$ and the impedance phase $\left(\phi^{TM}\right)$ of the TM polarization mode can be estimated as shown in Eq. (5) to Eq. (7).

$$\rho_a^{TM} = \frac{1}{w\mu}\left[Z_{TM}\right]^2 \tag{5}$$

$$Z_{TM} = \frac{\left(\frac{1}{\sigma - iw\varepsilon}\frac{\partial H_x}{\partial z}\right)}{H_x} \approx \frac{\left(\frac{1}{\sigma}\frac{\partial H_x}{\partial z}\right)}{H_x} \tag{6}$$

$$\phi^{TM} = \tan^{-1}\left(\frac{Imaginary\ \left[Z_{TM}\right]}{Real\ \left[Z_{TM}\right]}\right) \tag{7}$$

Generally, the relationship among h (along the z axis), f and ρ, which produced the skin depth of investigation or the depth of penetration of the EM waves in Eq. (8) can be compared with Eq. (5).

$$h \approx 503\sqrt{\frac{\rho}{f}} \tag{8}$$

The PQWT is designed to measure the electric potential difference at the middle of the M and N electrodes, which correspond to distinct depths of investigation as shown in Eq. (10). Therefore, the electric potential difference and depth are the output parameters by the equipment. The EM electrical method is best adapted for the two-dimensional imaging of near-surface structures because of its resolution, simplicity, easy to use, high penetrating depth and high sensitivity.

The Schlumberger configuration was adopted in this study. Fifteen VES points were occupied randomly at the dumpsite (Fig. 1d). In Schlumberger configuration, the inner (potential) electrodes (M and N) are maintained relatively constant, while the outer (current) electrodes (A and B) are successively increased outwardly with respect to the mean point of the inner electrodes [3]. Measurement was taken at each successive location of the outer electrodes. The SAS 4000 ABEM resistivity meter was programmed on the field in order to repeat measurements up to 4 times at each location, whereby the mean of these results was recorded for that point. The currents injected into the subsurface in this study varied from 20 to 100 mA [21, 22]. As a result of the extent of the study location, a maximum of 130 m current electrode spacing (AB) was achieved. It was ensured that the electrodes were firmly hammered to the ground during the survey and all the connecting cables were rightly connected to the appropriate knots.

In theory, the apparent resistivity (ρ$_a$) is the product of the geometric factor (G) and the resistance of individual lithology as presented in Eq. (9).

$$\rho_a = GR \tag{9}$$

Since the equipment used in this study is capable to process the ρ$_a$ automatedly, the mean ρ$_a$ recorded at each point was processed via a semi-automated approach known as partial curve matching [22]. The initial layer's parameters obtained were used to produce the final

resistivity curves by the WinResist program. The WinResist is a one-dimensional forward modeling package that uses an inversion program. Its advantage over other programs that process the VES data is that it has the ability to accommodate the manual curve matching's results with the ρ_a data prior to the display of the final modeled curves, which will be used for lithological characterization along the subsurface vertical axis [14]. The root mean square (RMS) error gotten for each VES point was below 10.0 in order not to over-filter the output parameters, since the study area is an active dumpsite that contains some dielectrics. The integrity of the confining media above the aquiferous zone was assessed based on the lithological composition within the topsoil and the overlying materials above the aquifer [23, 24].

The difference between the sounding configurations in the natural EM field and the conventional VES is that there are no A and B electrodes in the former. Despite the measurement point in the two configurations being at the mid-point, the M and N movements in the natural EM field survey are similar to that of the Wenner configuration, with a constant electrode spacing of 10 m being chosen in most cases. Variation in the potential difference with depth at a specific sounding spot could be obtained, which can be used to determine the depth of the buried anomaly.

Two borehole logs acquired at the southeastern and southwestern parts of the study area (control points) were used to produce the litho-section of the subsurface. The borehole litho-sections were correlated with the geoelectrical parameters of each layer obtained from VES curves. The beauty of integrating a borehole log with the VES layers' parameters is to ascertain the integrity of the geological interpretation of each litho-structural unit [3, 14].

4 Results and discussion
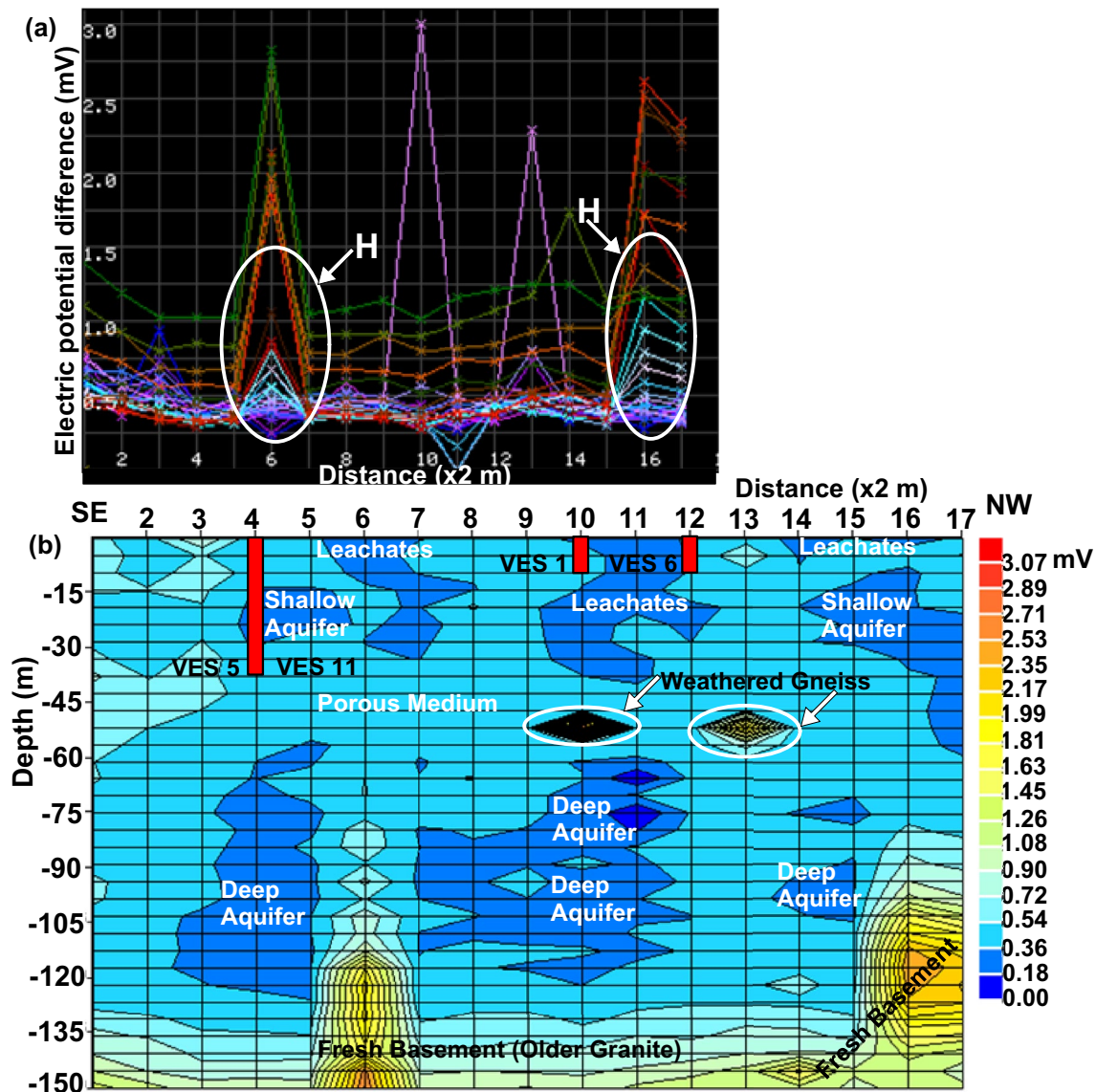
4.1 Natural electromagnetic field interpretation

The EM data acquired were processed and enhanced through automatic in-built software within the PQWT. The computation of data by the software is based on analogue to digital data sampling, which generates electrical potential difference curves at different frequencies and a 2D profile map along a traverse. A point of intersection or a low convergence of electrical potential difference (in mV) curves corresponds to a porous medium filled with fluid or a weathered rock formation [10–13]. Meanwhile, a high divergence of electrical potential difference curves could indicate a highly resistive, highly compacted or hard rock terrain [9]. In EM prospecting, the penetration depth is dependent on the electrical conductivity of the stratum and the frequency at which the EM field is propagating

[12]. The amplitude of the EM field decreases exponentially as it penetrates the subsurface, which in turn increases the penetration depth as the EM frequency and the conductivity of the stratum decrease [12].

The EM traverse 1 (Tr1) covers a length of 34 m (corresponding to 17 data points), which runs from southeast to northwest direction. Divergence of electrical potential difference curves (H) was noticed at distances 12 and 32 m in Fig. 2a. This could be interpreted as a hard rock formation or a basement rock, which attenuates the penetration depth of EM signals in a crystalline basement environment. In Fig. 2b, the traverse is composed of soft-to-medium subsurface formations. Generally, on the 2D EM map, low electrical potential differences could infer subsurface materials with low resistivity (or high conductivity) values, low-density values, porous medium and a zone of high potential for groundwater exploitation; while high electrical potential differences could depict subsurface formation with high resistivity values, high-density values and a layer with high potential for civil engineering structures [13]. The soft layer's depths varied from 80 to 135 m. The soft layer could be interpreted as a porous formation with high electrical conductivity, such as clayey formation, weathered rocks, sediments or decomposed organic matter from the dumpsite [6]. A shallow aquifer with varying depths from 15 to 30 m was identified at distances of 8 to 10 m on Tr1. Meanwhile, three prolific deep aquifers were present at depths > 60 m on Tr1. Migration of leachates from the surface to a depth > 30 m (beyond the depth of the shallow aquifer) was identified on Tr1. Consumption and usage of water from the shallow aquifer (that is, hand-dug wells) for domestic purposes around the dumpsite could be harmful, as a result of the depth of migration of leachates on Tr1 [6, 8], because leachate's pathways to aquifers are chiefly governed by gravity [25]. It permits leachates to flow vertically and laterally within the subsurface until it's able to interact with the nearest aquifer along the flow path [3]. Within the soft medium, there are two resistive intrusive bodies at distances of 20 and 26 m. These intrusive bodies at about 50 m depth could be interpreted as isolated weathered gneisses [26]. Beneath the soft formation lies the medium formation (Fig. 2b), which could be interpreted as the fresh basement (Older granite).

The Tr2, which was surveyed at the northwestern part, runs through a distance of 18 m, with data points of 9. The orientation of the second traverse moves from southwest to northeast (Fig. 1d). A steady homogeneous trend is observed on the electrical potential difference curves all through the Tr2, except at point 6 (distance 12 m) where H is observed (Fig. 3a). This corresponds to a high resistive intrusive body (isolated weathered gneiss) being observed at about 60 m depth in Fig. 3b. The Tr2 is composed of

Fig. 2 Natural electromagnetic field **a** Potential difference curves at varying frequecies along traverse 1 **b** 2D subsurface imaging for traverse 1 with nearby VES points

very soft-to-soft subsurface formations. A very soft layer is observed throughout the Tr2 and extends beyond 100 m depth. This could infer that communication exists between the leachates and the aquiferous medium within the northwestern axis of the study area [27]. The degree of conductive materials within the first layer in Tr2 could be an effect of a fluid-filled fault at the back of the dumpsite [17]. Water from boreholes and hand-dug wells at the upper axis of the study area could be harmful to humans for consumption and usage as a result of these conductive materials. The general subsurface pattern as revealed in Fig. 3b depicts two different conductive formations. The subsurface image on Tr2 revealed that there exist

aquifer-leachate interactions at the upper (northwestern and northern) axis of the study area.

The third traverse (Tr3), which is domiciled in the northern part, extends to a length of 22 m, corresponding to 11 data points. It trends in the southwest to northeast orientation (Fig. 1d). There are some scattered electrical potential difference curves on Tr3, with H being noticed at point 2 and point 10 (Fig. 4a). The scattered lines could be an effect of buried dielectric materials on the dumpsite. Meanwhile, the effect of H in Fig. 4a could be a result of the presence of shallow intrusive bodies being observed at depths 5 to 30 m on point 2 and points 9 to 11 in Fig. 4b. The subsurface patterns of Tr1 and Tr3 resemble each other. As depicted in the first traverse, the two layers
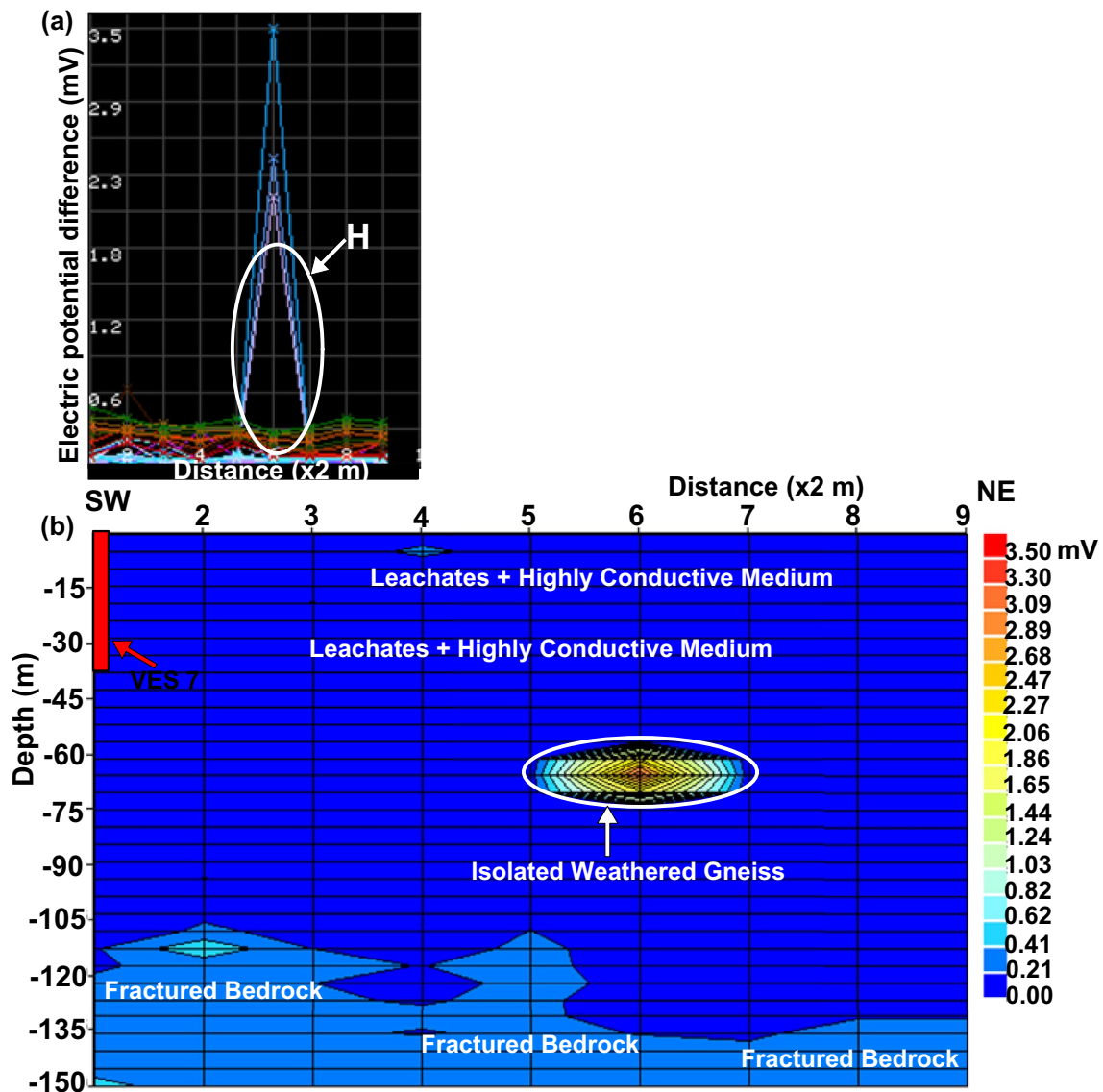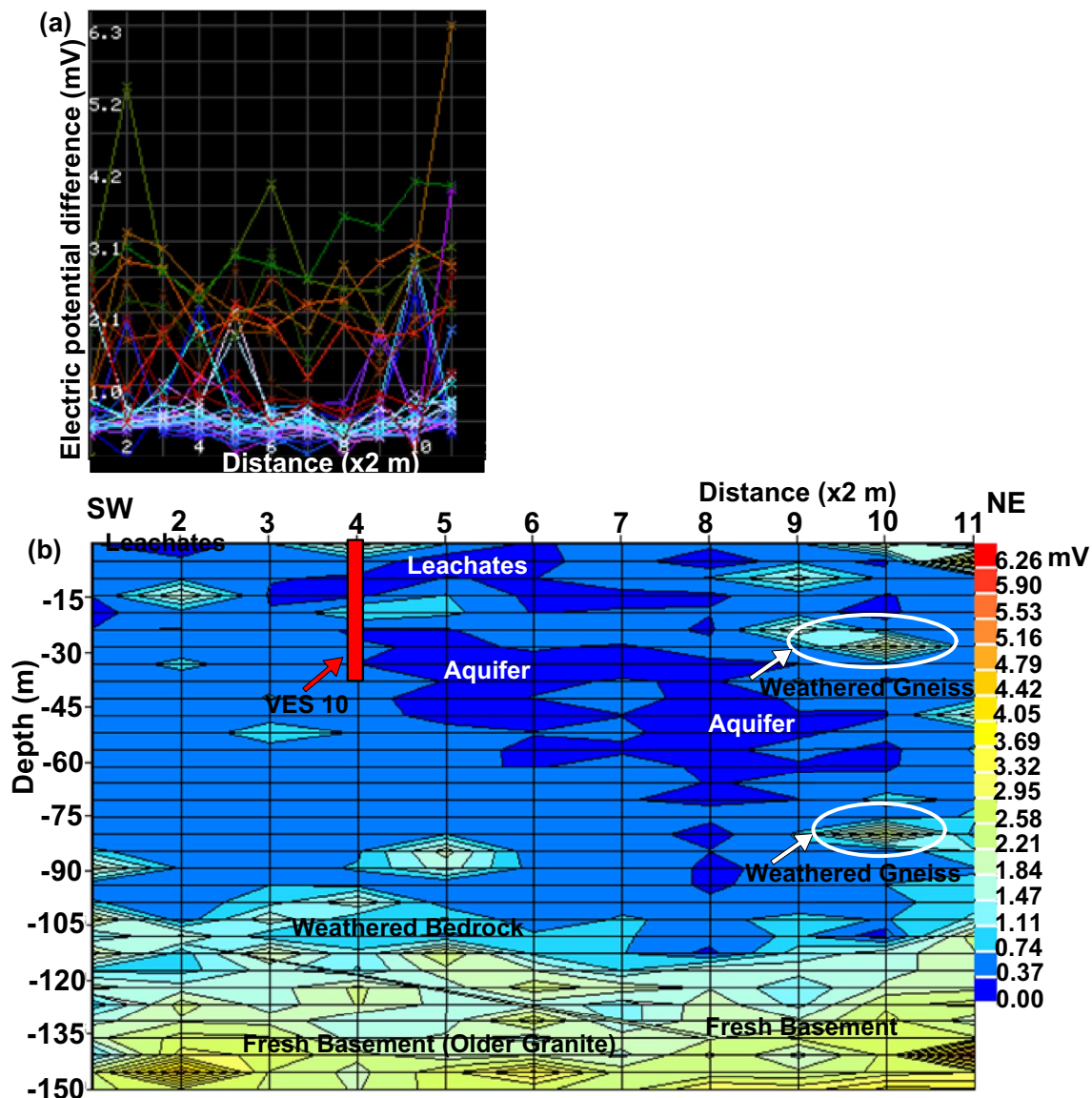
Fig. 3 Natural electromagnetic field **a** Potential difference curves at varying frequecies along traverse 2 **b** 2D subsurface imaging for traverse 2 with VES 7

present in Tr3 are composed of soft-to-medium formations as well. The depth of the soft formation is ≈ 100 m. Within the soft layer, a major aquifer is observed. The aquifer extends from point 4 to point 10 at depths of 25 to 70 m. A pocket of leachates overlying the aquifer is noticed at an approximate depth of 20 m. It is essential to set a time-lapse geophysical monitoring system on Tr3 to ensure that the people living around the northern axis of the study area are not abstracting water from contaminated aquifers [28]. An integration of weathered rock and a fresh basement (Older granite) constitute the medium formation, which lies beneath the soft layer in Tr3. The granitic layer is observed at an approximate depth > 105 m. Generally, granites of various ages have been found as intrusive

bodies among the underlying rocks (such as metasediments, migmatites and gneisses) of the crystalline basement rocks in Nigeria [29].

The Tr4 was surveyed towards the northeastern part of the study area. It trends from northwest to southeast orientation. The total traverse length of Tr4 is 20 m (which corresponds to 10 data points). Two distinctive patterns were formed on the graph (Fig. 5a). Some of the electrical potential difference lines were converged at the base, while other signals were spread out of the plot area with one H being noticed on the traverse (Fig. 5a). The output of the electrical potential difference responses resulted to three layers formations being observed on Tr4. These formations are soft-to-medium-to-hard subsurface layers

Fig. 4 Natural electromagnetic field **a** Potential difference curves at varying frequecies along traverse 3 **b** 2D subsurface imaging for traverse 3 with VES 10

(Fig. 5b). A thin soft layer (or sediments), which is interpreted as a thin overburden is present at depth < 5 m on the 2D map. It indicates that the waste disposal's effects are minimal at the northeastern axis of the fourth traverse. Within the medium layer (which is interpreted as a weathered zone), about four prolific aquifers were identified towards the end of Tr4 at varying depths from 15 to 20 m, 35 to 45 m and 50 to 70 m, respectively. Some aquiferous zones were also noted in the middle of Tr4 at a depth of 75 m (point 5) and depths of 55 to 65 m (point 6), respectively. There is no form of leachate-groundwater interaction on Tr4, which confirmed that the rate of migration of leachates into the aquifer system at the northeastern axis

of the study site is extremely low. The hard layer, which is interpreted as fresh basement rocks, is the third formation on Tr4. The basement rocks are noticed as intrusive bodies within the weathered layer (varying from 15 m to approximately 85 m depth), but are more pronounced at the vertical plane beyond 90 m. The basement pattern on Tr4 indicates that there are near-surface outcrops on this traverse.

The Tr5, which is the control, is located in the southwestern part of the study area. The traverse is located about 200 m away from the dumpsite. The orientation of Tr5 runs from northeast to southwest, with a total distance of 38 m (corresponding to 19 data points).
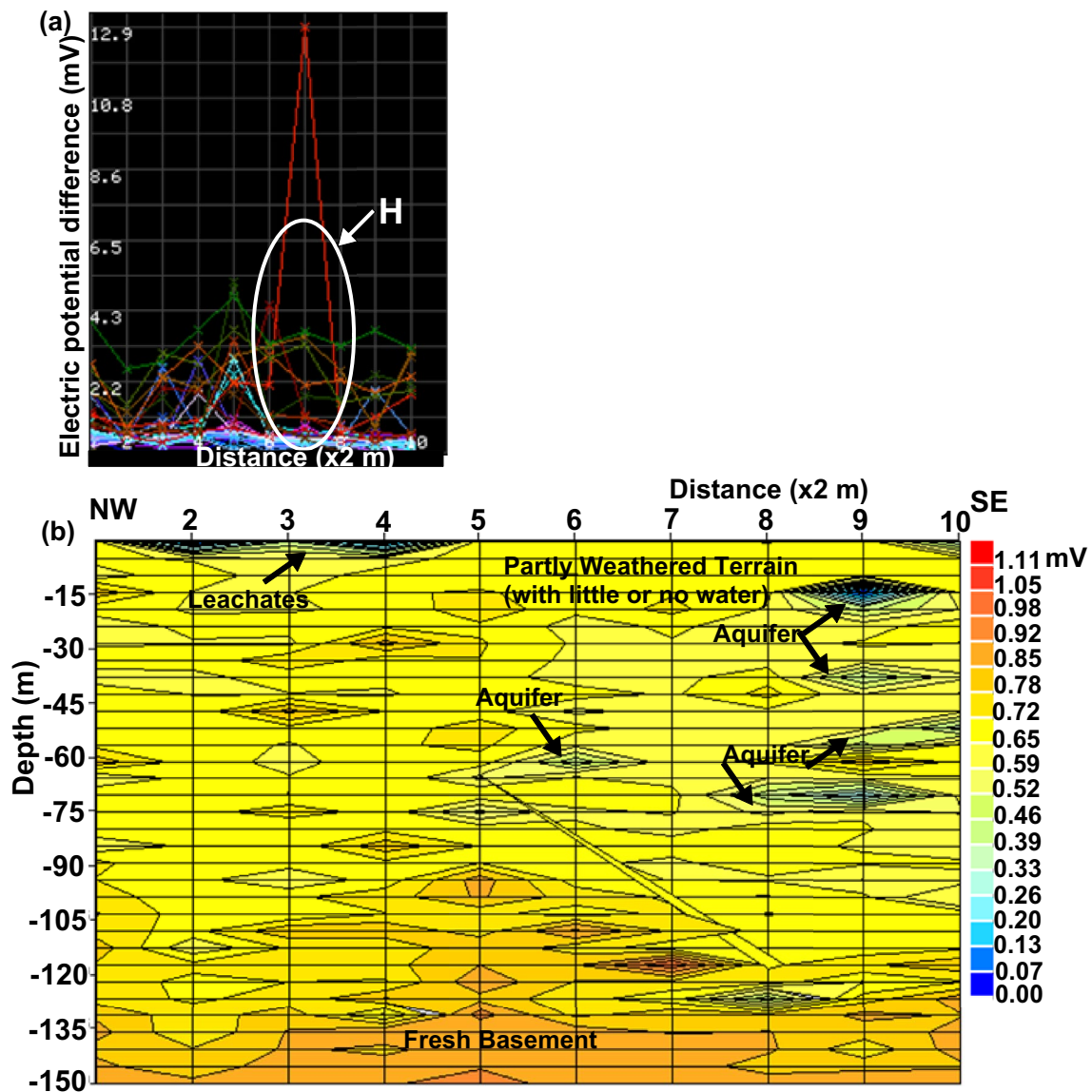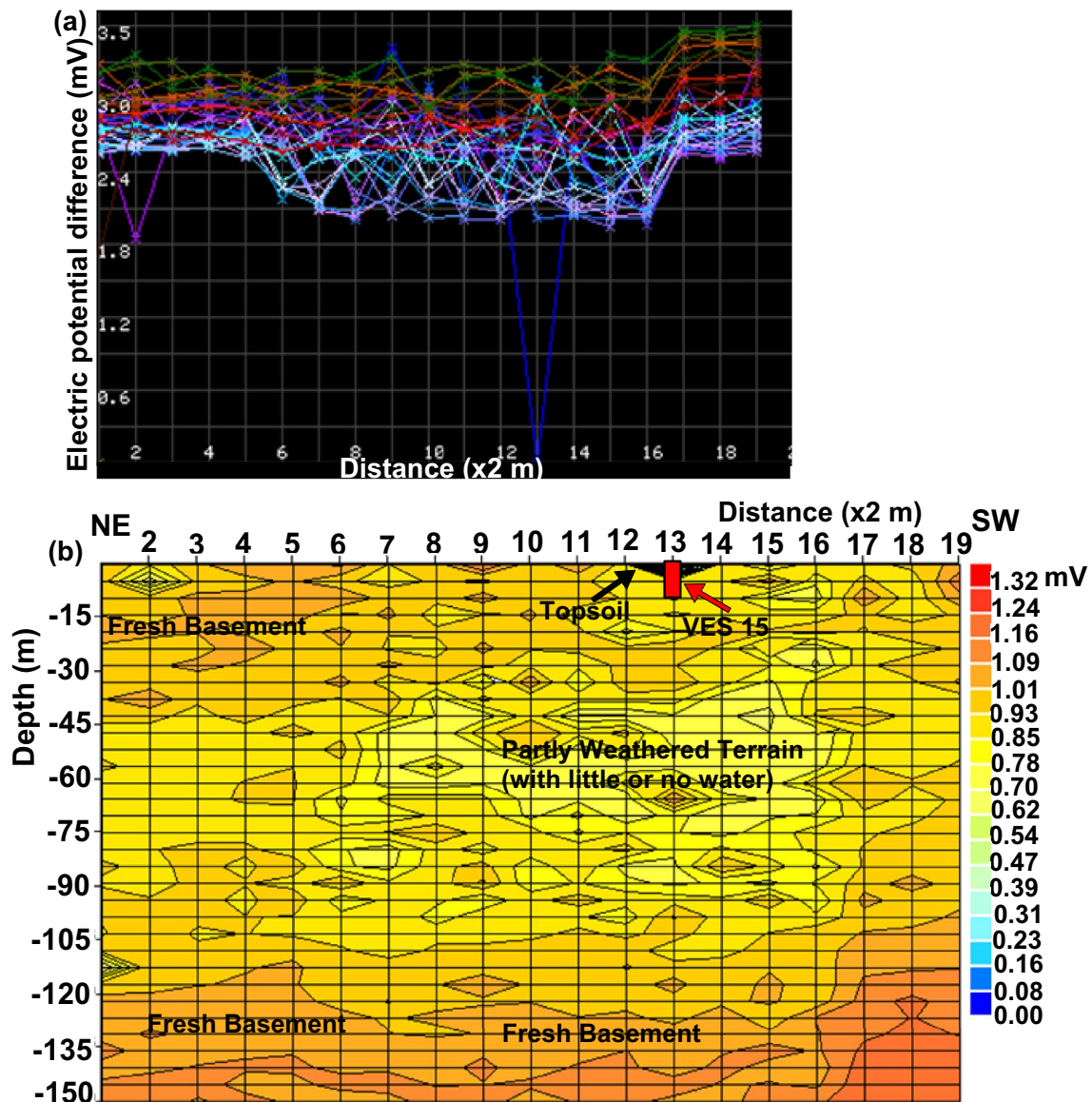
Fig. 5 Natural electromagnetic field **a** Potential difference curves at varying frequecies along traverse 4 **b** 2D subsurface imaging for traverse 4

The electrical potential difference lines are of an irregular pattern (Fig. 6a), which shows that the EM signals encountered some obstructions (such as hard terrain) that attenuate the EM signals on the traverse. The Tr5 is predominantly controlled by a very hard subsurface formation, with some outcrops at point 4 to point 6 and point 19 (Fig. 6b). These outcrops are observed close to the control traverse during the geophysical field work. A moderately weathered terrain is observed at the center of the traverse. The weathered zone extends laterally from distances 11 to 33 m and vertically from depths 40 to 90 m. There is an insignificant or low groundwater potential at about 5 m depth on point 2 and point 13 (Fig. 6b). These locations could only be utilized for hand-dug wells. There is a regular subsurface pattern on Tr4 and Tr5, which suggested that without the effect of the dumpsite, thick weathered rocks and fresh basement/bedrock constitute the study area. These two traverses (Tr4 and Tr5) are mainly characterized by high-resistivity and high density values which are the attributes of a hard or competent subsurface formation [20].

The locations (as shown in Fig. 1d) and the depths to bedrock of some VES points that are close to the EM traverses are revealed in Fig. 2b, Fig. 3b, Fig. 4b and Fig. 6b, respectively. Placement of the VES points to their relative positions on the EM traverses would assist to infer if there is a comparison between the FSM and VES results in terms of lithology. It is obvious that the depth

Fig. 6 Natural electromagnetic field **a** Potential difference curves at varying frequecies along traverse 5 (control) **b** 2D subsurface imaging for traverse 5 (control) with VES 15

of investigation for the FSM is far greater than that of the geoelectrical sounding technique. The relationship between the adopted methods will be revealed in the next Subsection.

4.2 Geoelectrical interpretation

Seven various geoelectrical sounding curve types were observed from automated processing of randomly sampled 15 VES points acquired on the dumpsite. A few of the obtained VES curves are shown in Fig. 7a–d. Lithological classifications of the geoelectrical sequences in the study area are mainly based on qualitative and quantitative

parameters from the observed VES curves [14, 22]. As reported by Adagunodo et al. [15], subsurface hydrological conditions could be deduced from qualitative interpretations. It has been established by Olawuyi and Abolarin [30] that a linear relationship exists between predicted borehole depths from VES curves and the actual borehole depths from the drilling logs. The subsurface geosounding parameters such as the number of layers, curve type, layer's resistivity, thickness, depth and lithological interpretations for each VES point are presented in Table 1. The processed curves revealed that 26.7% are of AA type; 13.2% are of HAK type; 6.7% each of KHK, KHAA and KHA types; while 20% each of HA and HAA types.
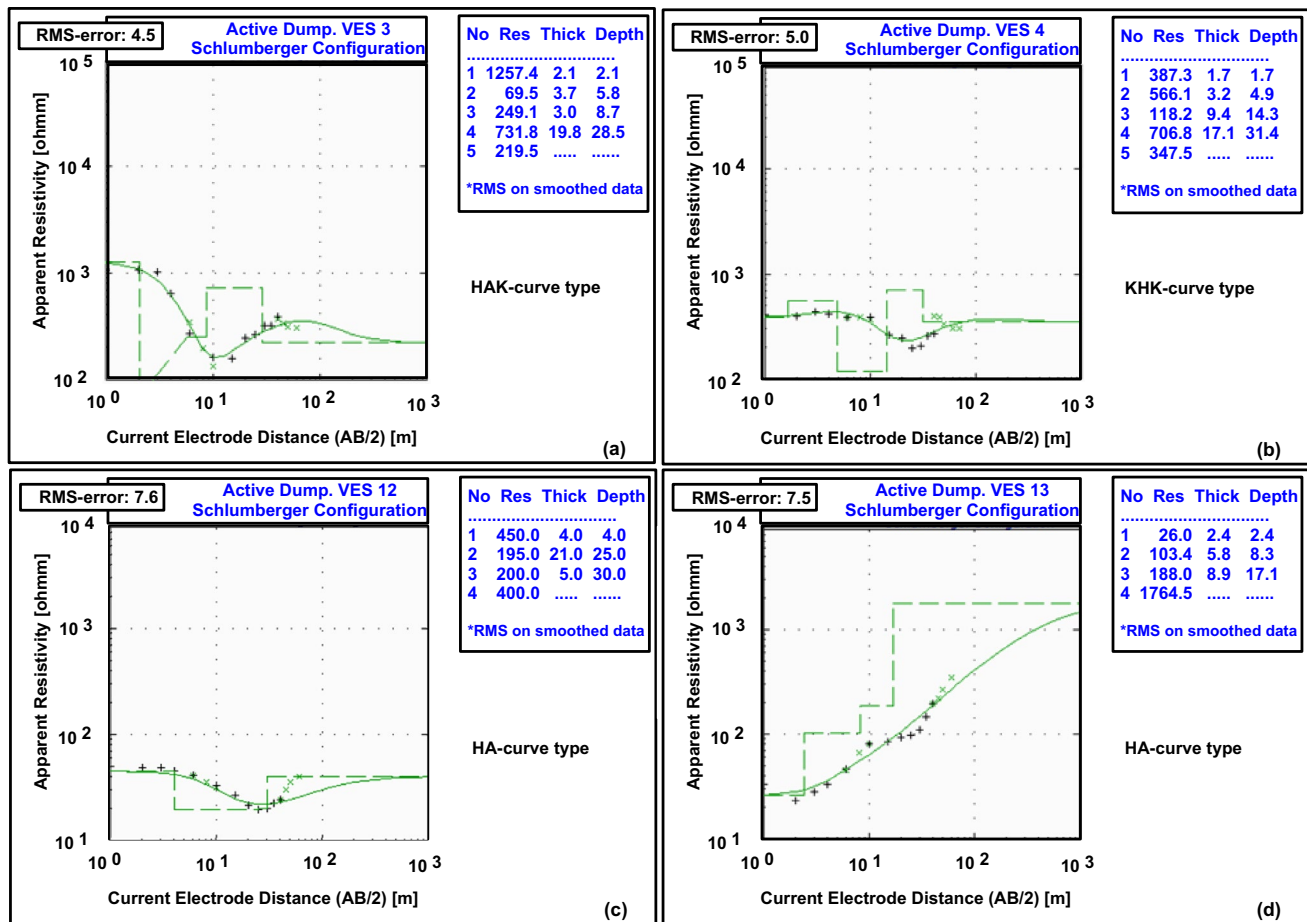
Fig. 7 Selected modeled curves from the study area **a** VES 3 **b** VES 4 **c** VES 12 and **d** VES 13

Correlations of logs for borehole (BH) data, VES points and EM traverses are presented in Fig. 8a, b. The available BH logs within the study area were correlated with the layers' parameters from VES results and the 2D imaging maps from the EM technique. The essence of the correlation is to reveal if there is synergy among the litho-structural sequences obtained from one method to the other in the study area. In some cases, the resistivity value of a particular layer could be observed in another subsequent layer (as in the present study), and the geological settings of the area of interest would be used as a guide to characterize the litho-facies in that domain [14]. In the same context, the geological background of the area of study is required when interpreting the litho-facies on the 2D map of the FSM. Moderate correlations exist between the BH 1, VES 15 and EM Tr5 in Fig. 8ai as well as BH 2 and VES 8 in Fig. 8aii. Apart from the lower saprock that could not be correlated in Fig. 8ai, there is synergy between the lithological units of BH 2 and VES 8 (in Fig. 8aii) and the depths of the conductive media that were mapped by VES and EM in Fig. 8a and b. The correlations showed that nearly same saprolites

(but at varying formation depths) are present both at the control points (towards the SW and SE) and on the main dumping zone (NW and the northern parts) of the study area (see Fig. 1d). Relative depths to groundwater were predicted by both BH and VES at fresh basement and fractured bedrock (or lower saprock), respectively. Also, depths of leachates mapped by VES results correlate with the leachate's depths being imaged by the FSM results.

The observed litho-facies in the study area (see Table 1 and Fig. 9a–c) are topsoil, clay, sandy clay, upper saprock, lower saprock and bedrock. The topsoil's resistivity and thickness varied from 10.0 to 1257.4 Ωm and 0.9 to 6.0 m, with mean values of 167.5 Ωm and 2.0 m, respectively. The composition of first layer (topsoil) is made up of decomposed organic bodies or clay and lateritic sand (Fig. 9a–c). The process of organic matter decomposition involves physical disintegration and biochemical evolution of complex living matter into uncomplicated biotic and abiotic molecules. Organic matter's decomposition is a dominant donor to ecosystem respiration, which controls the net emission of carbon from the ecosystem

Table 1 Obtained geoelectrical parameters from an active dumpsite

VES ID	No. of layers	ρ (Ωm)	h (m)	D (m)	Lithology	Curve type	Remark
1	4	15.1	1.6	1.6	Topsoil/decomposed sediments	AA	
		34.0	3.7	5.3	Clay/decomposed sediments		
		62.4	3.7	9.0	Upper saprock		
		3385.5	–	–	Bedrock		
2	4	22.0	1.0	1.0	Topsoil/decomposed sediments	AA	
		50.0	5.0	6.0	Clay/decomposed sediments		
		275.0	29.0	35.0	Upper saprock		
		395.0	–	–	Lower saprock		
3	5	1257.4	2.1	2.1	Topsoil/laterites	HAK	
		69.5	3.7	5.8	Clay/decomposed sediments		
		249.1	3.0	8.7	Sand clay/decomposed sediments		
		731.8	19.8	28.5	Upper saprock		
		219.5	–	–	Lower Saprock		
4	5	387.3	1.7	1.7	Topsoil/sand	KHK	
		566.1	3.2	4.9	Laterites (Near-surface intrusion)		
		118.2	9.4	14.3	Sand clay/decomposed sediments		
		706.8	17.1	31.4	Upper saprock		
		347.5	–	–	Lower saprock		
5	5	33.0	1.0	1.0	Topsoil/decomposed sediments	HAK	
		18.0	3.0	4.0	Clay/decomposed sediments		
		80.0	6.0	10.0	Sand clay/decomposed sediments		
		322.0	30.0	40.0	Upper saprock		
		179.0	–	–	Lower saprock		
6	4	19.6	1.3	1.3	Topsoil/decomposed sediments	AA	
		35.8	5.1	6.4	Clay/decomposed sediments		
		234.1	4.5	10.9	Upper saprock		
		2580.2	–	–	Bedrock		
7	6	19.0	1.0	1.0	Topsoil/decomposed sediments	KHAA	VES point at the NW zone
		50.0	5.0	6.0	Clay/decomposed sediments		
		33.0	4.0	10.0	Clay/decomposed sediments		
		64.0	10.0	20.0	Clay/decomposed sediments		
		168.0	20.0	40.0	Upper saprock		
		215.0	–	–	Lower saprock		Borehole at depth > 40 m
8	5	19.9	0.9	0.9	Topsoil	HAA	Control point at the SE zone
		5.5	1.8	2.8	Clay		
		6.6	7.3	10.1	Clay		
		24.5	4.0	14.1	Upper saprock		
		1113.3	–	–	Bedrock		
9	4	10.0	6.0	6.0	Topsoil/decomposed sediments	AA	
		25.0	19.0	25.0	Clay/decomposed sediments		
		29.0	15.0	40.0	Upper saprock		
		309.0	–	–	Lower saprock		
10	5	11.0	1.0	1.0	Topsoil/decomposed sediments	HAA	VES point towards the NW zone
		6.0	5.0	6.0	Clay/decomposed sediments		
		11.0	9.0	15.0	Sand clay/decomposed sediments		
		32.0	25.0	40.0	Upper saprock		
		90.0	–	–	Lower saprock		Borehole at depth > 40 m
11	5	43.0	3.0	3.0	topsoil/decomposed sediments	HAA	
		27.0	3.0	6.0	Clay/decomposed sediments		
		74.0	4.0	10.0	Sand clay/decomposed sediments		

Table 1 (continued)

VES ID	No. of layers	ρ (Ωm)	h (m)	D (m)	Lithology	Curve type	Remark
		400.0	30.0	40.0	Upper saprock		
		476.0	–	–	Lower saprock		
12	4	450.0	4.0	4.0	Topsoil/decomposed sediments	HA	
		195.0	21.0	25.0	Sand Clay/decomposed sediments		
		200.0	5.0	30.0	Upper saprock		
		400.0	–	–	Lower saprock		
13	4	26.0	2.4	2.4	Topsoil/decomposed sediments	HA	
		103.4	5.8	8.3	Sand clay		
		188.0	8.9	17.1	Upper saprock		
		1764.5	–	–	Bedrock (vertical intrusion)		
14	5	26.0	2.0	2.0	Topsoil/decomposed sediments	KHA	
		54.0	4.0	6.0	Clay/decomposed sediments		
		45.0	4.0	10.0	Sand clay/decomposed sediments		
		98.0	25.0	35.0	Upper saprock		
		236.0	–	–	Lower saprock		
15	4	173.0	1.0	1.0	Topsoil	HA	Control point at the SW zone
		49.0	3.0	4.0	Clay		
		80.0	6.0	10.0	Upper saprock		
		588.0	–	–	Lower saprock		

N.B: ρ indicates resistivity, h indicates thickness, D indicates Depth

in conjunction with the aid of photosynthesis [31]. As beneficial as the decomposed organic matter is to the ecosystem, it becomes toxic when the decomposed organic medium leaches into the aquifer [32]. Aquifer contamination is a long-lasting risk, because the degradation of waste continues for years after the waste has been dumped and decomposed, leading to the potential migration of leachates that could percolate and contaminate the groundwater systems (that is, the aquiferous media) [33]. The extent of accumulated leachates in the aquifer is controlled by the following environmental factors: precipitation, groundwater flow, geology of the area of interest which dictates the subsurface permeability, leachate infiltration rate and the groundwater piezometric head [34]. When a layer that is mixed with decomposed organic bodies overlies the aquifer unit, consumption of water from the affected region becomes a threat to the user's lives, because the medium would be highly porous with limited interconnectivity of pore spaces [31, 33]. Decomposed organic matter and clay, being one of the highly conductive media, are characterized by resistivity below 100 Ωm [35]. Under the influence of rainfall over time, leachates percolate into the aquifer which makes the shallowest aquifer unfit for consumption. 73.3% of the topsoil is composed of the clayey formation (with $\rho_a < 100$ Ωm), while the remaining 26.7% is composed of the lateritic sand formation (with

$173 \leq \rho_a \leq 1257$ Ωm). This indicates that more than two-third of the topsoil is polluted.

The resistivity and thickness of the second layer varied from 5.5 to 566.1 Ωm and 1.8 to 21.0 m, with mean values of 85.9 Ωm and 6.1 m, respectively. The second layer is composed of decomposed organic matter (or clay) and a mixture of humus with sediments (or sandy clay) formations, with 80% of this layer being made up of decomposed organic sediments (Fig. 9a–c). Extensions of the second layer's formations are observed in the third and fourth layers respectively. 53.3% and 6.7% of the total sounded points exhibit third and fourth layers (Table 1). The resistivity and thickness of the third layer varied from 6.6 to 249.1 Ωm and 3.0 to 9.4 m, with mean values of 77.1 Ωm and 5.8 m, respectively. VES 7 is the only geoelectrical model with 6 lithological units. The resistivity and thickness of the fourth layer for VES 7 are 64 Ωm and 10 m, respectively. The upper geoelectrical sequences (from layer 1 to layer 4) revealed that there are migrations or percolations of leachates to depths varying from 4.0 to 25.0 m. This zone is depicted by the leachates-aquifer interphase in Fig. 9a–c. The depths of leachate's migration in this study correspond to the result obtained by Ugbor et al. [3] showed that the leachate-aquifer mixing occurred at 21.7 m depth.

The resistivity and thickness of the fifth layer varied from 24.5 to 731.8 Ωm and 3.7 to 30.0 m, respectively. The fifth layer is named the upper saprock, because it is composed of a weathered medium [36], which constitutes
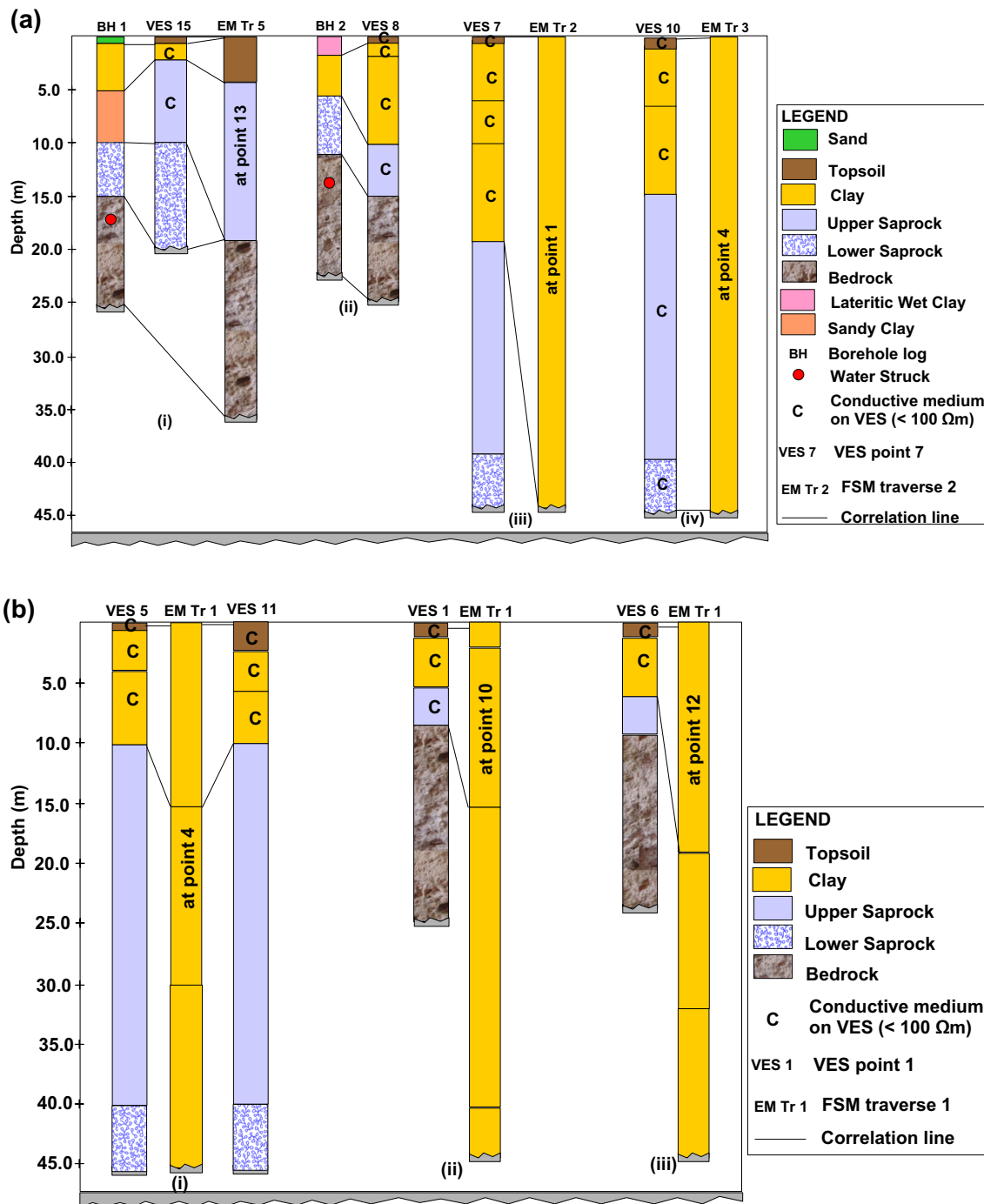
Fig. 8 **a** Correlations of logs for (i) BH 1, VES 15 and EM Tr5$_{point\ 13}$ (ii) BH 2 and VES 8 (iii) VES 7 and EM Tr2$_{point\ 1}$ (iv) VES 10 and EM Tr3$_{point\ 4}$. **b** Correlations of logs for (i) VES 5, EM Tr1$_{point\ 4}$ and VES 11 (ii) VES 1 and EM Tr1$_{point\ 10}$ (iii) VES 6 and EM Tr 1$_{point\ 12}$

the first aquifer system (Fig. 9a–c). Weathering of rocks is instrumental in the accumulation of water in the crystalline basement aquifer. It tends to remodel the petrographic constituents and physical properties of the crystalline basement rocks [26]. Most rocks that are enriched in ferromagnesian minerals in SW Nigeria are susceptible to thick weathering, because the SW Nigerian climate is

tropical humid. The weathered medium is thickened in regions with high rainfall, as in the case of Ibadan which is observed in this study [26]. The depth of the first aquifer varied from 4.0 to 25.0 m, with a mean of 11.9 m. This indicates the tendency of leachate's mixing with groundwater at the first aquifer [33], which makes abstraction of
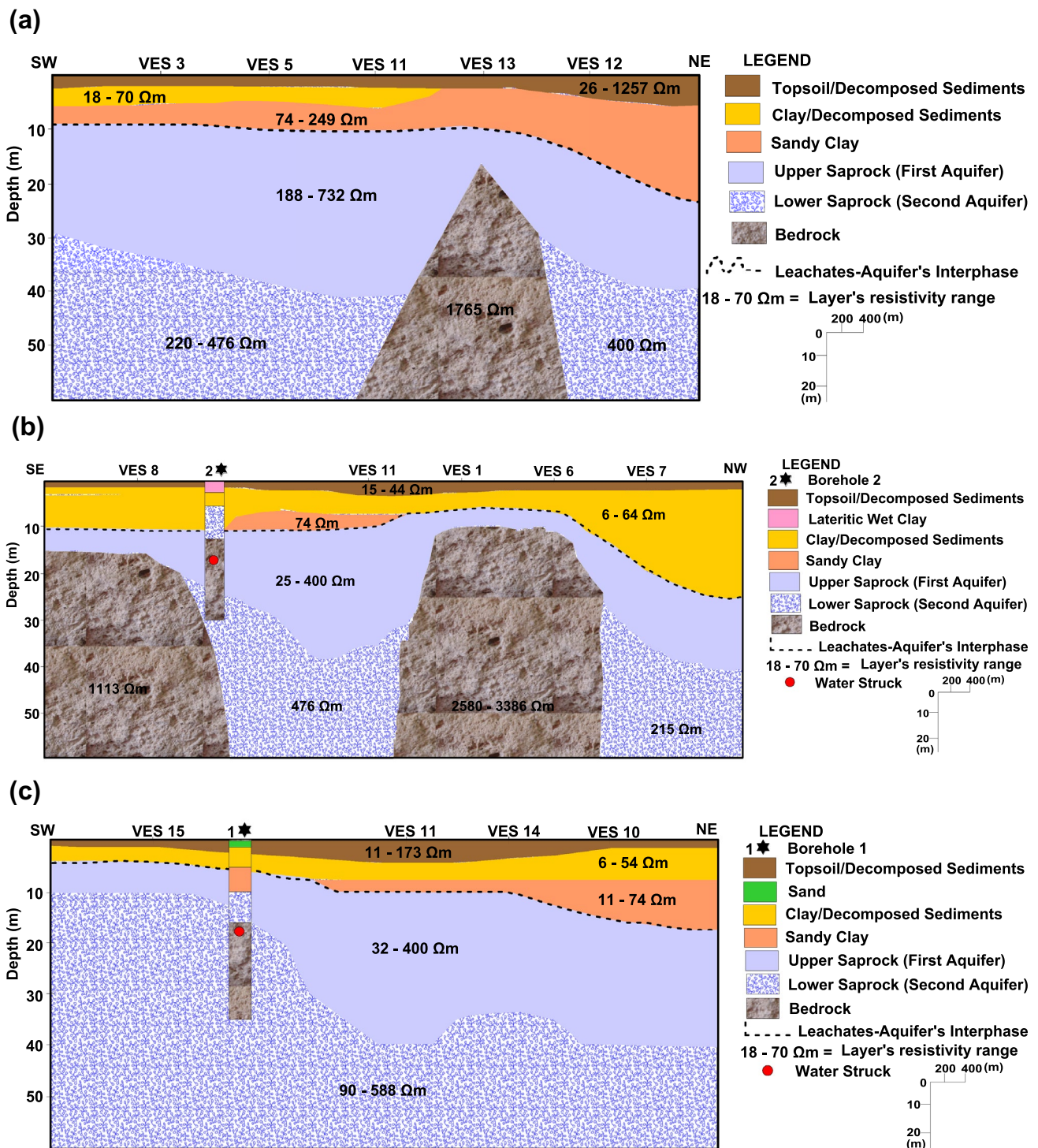
Fig. 9 **a** Geoelectric section of traverse 1.**b** Geoelectric section of traverse 2.**c** Geoelectric section of traverse 3

groundwater at the upper saprock unfit for consumption and other uses without treatment [6, 13].

The sixth layer is made up of both the lower saprock and the bedrock (Fig. 9a–c). The lower saprock is the fractured basement, while the bedrock depicts the fresh

basement. The fresh basement exhibits high resistivity due to the insignificant porosity and permeability of the medium [13, 14], which leads to its inability to store groundwater. Meanwhile, fracture density controls the hydraulic parameters of the fractured basement. In the

lower saprock, the rock pore spaces and their interconnectivity are enhanced, which leads to an increase in the groundwater storage capacity of the fractured basement [15]. The resistivity of the lower saprock is generally < 1000 Ωm [14, 15, 22], which signifies an accumulation of groundwater in the fractured basement. Apart from the climatic conditions, fracturing patterns and their permeability are essential in the accumulation of groundwater in the crystalline basement aquifer [26, 36]. The resistivity of the sixth layer and the depth-to-basement (that is, depth of the regolith) varied from 90.0 to 3385.5 Ωm and 9.0 to 40.0 m, with mean values of 819.9 Ωm and 28.0 m. The fractured basement shared 73.3% of the sixth layer (lower saprock and bedrock), which indicates that approximately three-quarter of the sixth layer is favourable for groundwater exploitation. The lower saprock constitutes the second aquifer, which is the safest medium to abstract groundwater for consumption and other uses in the study area [33].

To visualize the litho-facies in the study area, three geoelectric sections (GS) were produced (Fig. 9a–c). The GSs were constructed based on the linear point-to-point arrangement of some VES points. The three traverses were selected such that the subsurface lithological units were mapped from different orientations with respect to VES 11 (Fig. 1d). The first lithology that is common to the three GSs is the topsoil with varying resistivity from 26 to 1257 Ωm (Fig. 9a), 15 to 44 Ωm (Fig. 9b) and 11 to 173 Ωm (Fig. 9c). The topsoil is characterized by low-to-moderately high resistive portions, with low resistive signatures sharing more than two-third of the first layer. Beneath the topsoil lies another low resistive zone, which is classified as a clay formation. The second layer resistivity varied from 18 to 70 Ωm (Fig. 9a), 6 to 64 Ωm (Fig. 9b) and 6 to 54 Ωm (Fig. 9c). The first two layers are interpreted as zones of decomposed organic sediments [37]. The next underlying zone is also characterized by low-to-medium resistive signatures. The resistivity of the third layer varied from 74 to 249 Ωm in Fig. 9a, 74 Ωm in Figs. 9b and 11 to 74 Ωm in Fig. 9c, respectively. The third layer is composed of mixtures of humus and sediments, which is classified as a sandy clay formation.

From the three traverses, there is either a thin-out of the third layer at the beginning of the traverse (see Fig. 9b and c) or a thin-out of the second layer at the end of the traverse (see Fig. 9a). The lithology could be as a result of the slope or topography of the study area, which is responsible for the spread of the decomposed organic sediments on the dumpsite. The topsoil, second-layer and the third layer low resistivity values generally indicate the downward flow of leachates, as there is no evidence of a sealing medium that could inhibit the leachate's-to-aquifer mixing in the study area [27]. Geomembrane, which serves as an interphase between the polluted media and the first aquifer, shows that a thick saprolite exists at the end of each GS. This indicates that the leachates flow through the northeast, north and northwest directions. The synergy of the fluid flow results by EM and VES in this study has confirmed that the leachates percolate into the groundwater system through the fault network at the northwestern zone of the study area as reported by Adagunodo et al. [17].

The first aquifer overlies the last layer, with the resistivity of 188 to 732 Ωm at traverse 1, 25 to 400 Ωm at traverse 2 and 32 to 400 Ωm at traverse 3. The first aquifer is prone to contamination, because the plumes could migrate beyond the geomembrane zone over a significant time or by rain-water infiltration during the rainy season [27, 33]. Although, the diffusion process in groundwater is not as fast as that of surface water, it is advisable to exploit groundwater from the second aquifer so as to access safe water for consumption and other uses. To characterize the subsurface facies and to confirm the relative depth to groundwater in the study area, the available borehole logs were integrated with the GS of traverse 2 and traverse 3. The depth at which water was struck at traverse 2 coincides with the first aquifer system, while that of traverse 3 matches with the second aquiferous medium. There is a plausibility that leachates have infiltrated into the second borehole (i.e. BH 2).

To predict the groundwater potential and to produce the fluid dynamics maps of the study area, the overburden thickness (OT), bedrock resistivity (BR), coefficient of anisotropy (λ), reflection coefficient (RC), transmissivity (T), transverse resistance (TR) and bedrock relief were estimated from the VES parameters (such as thickness (h), resistivity (ρ) as well as the depth of two or more media) and other scientific relationships. The OT is the total thickness of the regolith overlying the bedrock. In a crystalline environment, the OT > 15 m is considered thick, which is viable for groundwater exploration [13]. The OT in the present study varied from 9.00 to 40.00 m, with 26.7% falling within the thin overburden category (Tables 2 and 3). The BR is the resistivity of the last lithologic unit. The BR < 1000 Ωm is regarded as fractured bedrock, while BR > 1000 Ωm is classified as fresh bedrock [19]. A combination of the thick overburden and fractured bedrock is an indicator of the development of secondary porosity and permeability in basement complex terrain [15]. The estimated BR in this study varied from 90.00 to 3385.50 Ωm (Table 3). About 73% of the entire bedrock is fractured. The λ was estimated using Eq. (10). Low values of λ depict low groundwater potential. The estimated λ from the current study varied from 1.04 to 1.56 (Table 3), which corresponds to the medium and good groundwater potential (Table 2).

Table 2 Groundwater potential standards and their inferences

OT (m)	Inference[1]	BR (Ωm)	Inference[2]	λ	Inference[3]	RC	Inference[4]	T (m²/day)	Inference[5]	TR (Ωm²)	Inference[1]
<15	Thin overburden	<1000	Fractured bedrock	<1.00	Poor GP	<0.8	High GP	>1000	Very high GP (High regional)	<5000	Poor GP
>15	Thick overburden	>1000	Fresh bedrock	1.00–1.50	Medium GP	>0.8	Low GP	100–1000	High GP (Low regional)	>5000	Good GP
				1.51–2.00	Good GP			10–100	Intermediate GP (Community and Industrial)		
				>2.00	Excellent GP			1–10	Low GP (Private or individual)		
								0.1–1	Very low (Low private access)		
								<0.1	Negligible GP		

N.B: *OT* Overburden thickness, *BR* Bedrock resistivity, *λ* coefficient of anisotropy, *RC* Reflection coefficient, *T* Transmissivity, *TR* Transverse resistance, *GP* Groundwater potential

1 = Alabi et al. [13], 2 = Adagunodo et al. [15], 3 = Sunmonu et al. [38], 4 = Bayewu et al. [39], 5 = Krasny [41]

80% of the calculated λ are classified within the medium groundwater potential domain.

$$\lambda = \sqrt{\frac{\sum_{i=1}^{n-1} h_i \cdot \rho_i \sum_{i=1}^{n-1} \frac{h_i}{\rho_i}}{\left(\sum_{i=1}^{n-1} h_i\right)^2}} \qquad (10)$$

where,

i is the summation limit ranging from order 1 to order n-1 (or the layer overlying the bedrock).

The integrity of the crystalline bedrock does not rely solely on the BR but on other parameters such as the RC and the T [39]. The RC was estimated using Eq. (11). The degree of the fracturing pattern of bedrock is revealed by distributions of the RC [24]. Zones with RC < 0.8 correspond to high groundwater potential zones. Integration of the RC < 0.8 with OT > 15 m and BR < 1000 Ωm are good prospects for high groundwater accumulation and fluid flow. The RC in the study area varied from -0.50 to 0.96, with one-third of the study site being covered with the RC > 0.8. The T describes the fluid flow rate in the entire aquifer system. There is a very high positive correlation among the T, aquifer thickness (h_a) and hydraulic conductivity (K) [40]. The K depicts the fluid flow rate per unit cross-sectional area. Both T and K are controlled by the rock's petrophysical parameters (such as volume of water, permeability, clay or shale contents and porosity). It implies that a high value of either T or K signifies high groundwater productivity. The T in this study was estimated using Eq. (12), which varied from 1.62 to 464.65 m².day^{-1} (Table 3). Based on the Krasny [41] ranking, the obtained classifications of T in the study area varied from low to high groundwater potential (Tables 2 and 3). It indicates that the groundwater system in the study area could serve an industrial purpose if properly exploited.

$$RC = \frac{\rho_n - \rho_{n-1}}{\rho_n + \rho_{n-1}} \qquad (11)$$

$$T = \left[\left(386.40 \times \left(R_{aq}^{-0.93283}\right)\right) \times h_a \right] \qquad (12)$$

where,

n is the bedrock (or nth) layer; R_{aq} is the resistivity of the aquiferous medium.

The TR is one of the Dar Zarrouk parameters that determine the hydraulic parameters. The connectivity between the groundwater flow from Darcy's law and electrical flow from Ohm's law is buttressed by the relationship between the Dar Zarrouk parameters and the T of an aquifer. The TR reveals that the direction of groundwater flow is perpendicular to the direction of electrical

Table 3 Groundwater potential from the inverted VES parameters

OT (m)	BR (Ωm)	λ	RC	T (m²/day)	TR (Ωm²)	GP
9.00	3385.50	1.14	0.96	4.58	380.84	Low yield
35.00	395.00	1.30	0.18	211.30	8247.00	High yield
28.50	219.50	1.45	− 0.50	464.65	18134.60	High yield
31.40	347.50	1.34	− 0.30	384.96	15667.30	High yield
40.00	179.00	1.53	− 0.30	263.95	10227.00	High yield
10.90	2580.20	1.56	0.83	27.05	1261.51	Intermediate yield
40.00	215.00	1.23	0.12	80.87	4401.00	Intermediate yield
14.10	1113.30	1.20	0.96	1.62	173.99	Low yield
40.00	309.00	1.07	0.83	7.43	970.00	Low yield
40.00	90.00	1.22	0.48	13.93	940.00	Intermediate yield
40.00	476.00	1.56	0.09	342.05	12506.00	High yield
30.00	400.00	1.04	0.33	24.90	6895.00	High yield
17.10	1764.50	1.25	0.81	41.16	2335.32	Intermediate yield
35.00	236.00	1.08	0.41	53.08	2898.00	Intermediate yield
10.00	588.00	1.07	0.76	10.00	800.00	Intermediate yield

N.B: *OT* Overburden thickness, *BR* Bedrock resistivity, *λ* coefficient of anisotropy, *RC* Reflection coefficient, *T* Transmissivity, *TR* Transverse resistance, *GP* Groundwater potential
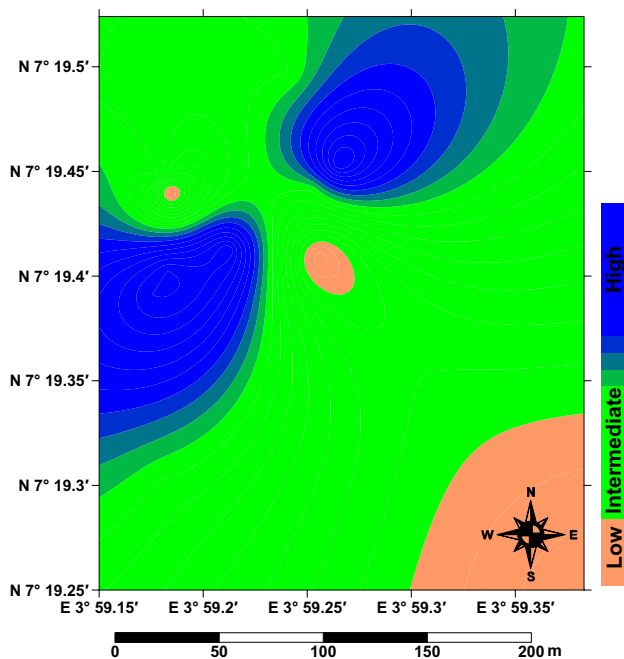
Fig. 10 Inferred groundwater yield from the study area

current flow in the aquiferous medium. Meanwhile, the longitudinal conductance, which was not considered in this study, explains that the groundwater flow direction is parallel to the electrical flow direction [40]. The TR in this study was estimated using Eq. (13). The estimated TR varied from 173.99 to 18,134.60 Ωm² (Table 3). Zones with low TR depict locations with low aquifer thickness or media with the presence of fine-grain size materials

(such as clay or shale). Based on Alabi et al. [13], the TR < 5000 Ωm² is characterized by poor groundwater yield, while the TR > 5000 Ωm² depicts good groundwater yield (Table 2).

$$TR = \sum_{i=1}^{n-1} h_i \cdot \rho_i \tag{13}$$

The six groundwater parameters that were assessed in this study (as shown in Table 3) were juxtaposed with the revealed standards in Table 2 to produce the final groundwater yield map in Amuloko (see Fig. 10). The intermediate groundwater potential of the northwestern part in the study area further confirmed that the subsurface media are underlain by fine grain size materials (such as decomposed organic bodies or fluid-filled clayey formation), which is the most conductive region with thick regolith in the study area (as shown in Figs. 1d, 3, 4 and 9b). The most productive regions are the northern and the western zones of the study area. The low groundwater yield in the southeastern part supports the reason for the failure of the BH 2, whose log was used in this study. In summary, 20% of the study site shares a low groundwater yield, while 40% each share an intermediate and a high groundwater yield, respectively (Fig. 10).

The fluid flow in the subsurface is dependent on the pressure and subsurface elevation (hydraulic head). It flows from higher hydraulic head points to the lower points. In an unconfined aquifer, the hydraulic gradient can be described as the slope of the water table. Meanwhile, Condon and Maxwell [42] revealed that groundwater fluxes are controlled by topographic gradients, as

Fig. 11 Direction of flow of fluids in the study area
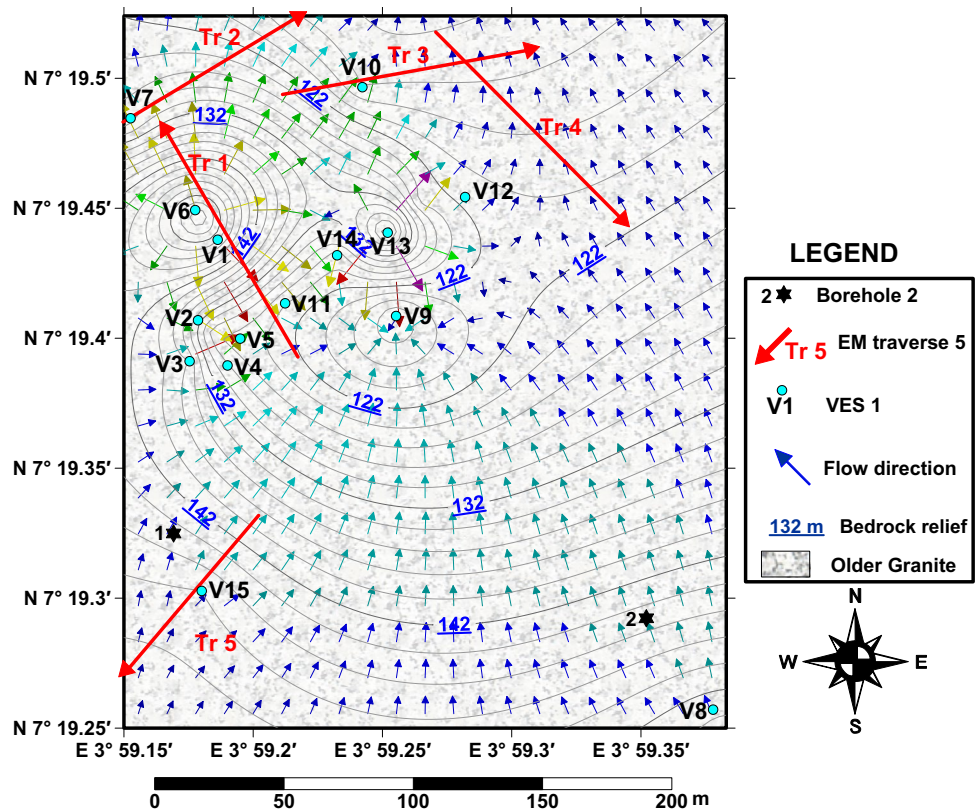
opposed to gradients in pressure head, in low conductivity, flat topography or high recharge environments. Further, the movement of groundwater in the subsurface is directly linked to the bedrock relief of the terrain [38]. To understand the direction of the fluid flow in the present study, the fluid dynamics map was produced from the bedrock relief signatures, which is a function of the surface elevation and the overburden thickness. Bedrock relief is used to image the bedrock topography, such that low topographic signatures would serve as collecting troughs while high signatures would serve as discharge points [38]. The directions of fluid flow were presented using vector lines (Fig. 11). The two observed fluid flow types in the current study are the non-uniform flow and the turbulent flow. The turbulent flow occurs at the central and northwestern zones, while the non-uniform flow is present at other regions. The directions of the fluid flow are in the S–N and SE–NW trends. The pattern of the vector lines showed that the hydrodynamics of the fluid is controlled by the topographic properties and the fault, which is observed at the northwestern part of the study site (see Fig. 1b). This fault, which trends in the NE–SW orientation, drains the fluid from the study site (granite gneiss geological formation) to the undifferentiated gneiss complex (see Fig. 1b). The fluid dynamics, however, justified the reason for the thick conductive materials being mapped at the northwestern and northern parts of the study area.

Integration of the VES parameters with the geologic information and hydraulic parameters in this sub-section has helped us to know the number of litho-structural units, the depth of infiltration of contaminants to the groundwater system and the fluid dynamics (of both leachates and groundwater) in the study area. Interpretation of VES data has not only been effective in groundwater exploration [14], near-surface bed characterization [43] and environmental studies [3]. It has been proven useful in the determination of fluid transmissibility, bedrock permeability, fluid salinity and fluid pathways in the subsurface.

5 Conclusion

Application of the natural EM field and geoelectrical sounding methods to assess the leachate's pathways in an active dumpsite has proven to be effective for geo-imaging of the near-surface conductive media. The conductive signatures at the near-surface are considered as the build-up terminals for contaminant's spreads into the aquifer. The depths of leachate's mixing into the aquiferous units at the western, northwestern and northern parts of the study area varied from 4.0 to 30.0 m. The leachate's-aquifer interaction being observed at the upper saprock in the present study has rendered the first aquifer, which is delineated at depths varying from 4.0 to 25.0 m, unfit for exploitation.

To access the contaminant free groundwater, it is advisable to explore the second aquifer (that is, lower saprock), which is delineated at depths varying from 9.0 to 40.0 m. The groundwater potential of the lower saprock revealed that 20% of the domain is characterized by low groundwater yield, while 40% of the medium is characterized by intermediate and high groundwater yield in each case. The western and the northern parts of the study area could be considered for drilling in case there is a need to develop a borehole for industrial purposes in the future. The directions of the fluid flow are in the S–N as well as SE–NW orientations. The hydrodynamics in this study could be linked to the fault towards the northwestern part of the study area. The fluid dynamics, however, justified the reason for the thick conductive materials being mapped at the northwestern and northern parts of the study area.

Author contributions TAA conceived, designed and supervised the study. Mobilization of the geophysical team for field-work was executed by TAA, AIO and POE. Data analysis and interpretation were performed by TAA, AIO and NOA. The first draft of the manuscript was written by TAA. All authors read and commented on previous versions of the manuscript and its approval for submission.

Data availability The data used to support the findings of this study are available on request through the corresponding author.

Code availability Not applicable.

Declarations

Competing interests The authors declare no competing interests.

Conflict of interest On behalf of all authors, the corresponding author states that there is no conflict of interest regarding the publication of this article.

Ethical approval Not applicable.

Consent to publication All authors gave their consent to publish this article.

References

1. Aladejana JA, Odeyemi OO, Tijani MN, Hassan I (2018) Integrated assessment of leachate concentration in soil underlying Amuloko open waste dumpsite, Ibadan southwestern. Niger J Min Geol 54(1):1–11
2. Adabanija MA, Alabi TO (2014) An integrated approach to mapping the concentration and pathway of leachate plumes beneath a dump site in south-western Nigeria. Int J Sci Eng Res 5(1):1565–1571
3. Ugbor CC, Ikwuagwu IE, Ogboke OJ (2021) 2D inversion of electrical resistivity investigation of contaminant plume around a dumpsite near Onitsha expressway in southeastern Nigeria. Sci Rep 11:11854. https://doi.org/10.1038/s41598-021-91019-3
4. Cozzarelli IM, Boehlke JK, Masoner J, Breit GN, Lorah MM, Tuttle MLW, Jaeschke JB (2011) Biogeochemical evolution of a landfill leachate plume, Norman, Oklahoma. Ground Water 49:663–687
5. Supandi S (2021) Geotechnical profiling of a surface mini waste dump using 2D wenner-schlumberger configuration. Open Geosci 13(1):335–344. https://doi.org/10.1515/geo-2020-0234
6. Olafisoye ER, Sunmonu LA, Ojoawo A, Adagunodo TA, Oladejo OP (2012) Application of very low frequency electromagnetic and hydro-physicochemical methods in the investigation of groundwater contamination at Aarada waste disposal site, Ogbomoso, Southwestern Nigeria. Aust J Basic Appl Sci 6(8):401–409
7. Bai D, Lu G, Zhu Z, Zhu X, Tao C, Fang J (2022) Using electrical resistivity tomography to monitor the evolution of landslides' safety factors under rainfall: a feasibility study based on numerical simulation. Remote Sens 14(15):3592. https://doi.org/10.3390/rs14153592
8. Park S, Yi M-J, Kim J-H, Shin SW (2016) Electrical resistivity imaging (ERI) monitoring for groundwater contamination in an uncontrolled landfill, South Korea. J Appl Geophys 135:1–7. https://doi.org/10.1016/j.jappgeo.2016.07.004
9. Oyegoke SO, Ayeni OO, Olowe KO, Adebanjo AS, Fayomi OO (2020) Effectiveness of geophysical assessment of boreholes drilled in basement complex terrain at Afe Babalola University, using electromagnetic method. Niger J Technol 39(1):36–41. https://doi.org/10.4314/njt.v3911.4
10. Yulong L, Tianchun Y, Tizro AT, Yang L (2023) Fast recognition on shallow groundwater and anomaly analysis using frequency selection sounding method. Water 15(1):96. https://doi.org/10.3390/w15010096
11. Yang TC, Gao QS, Li H, Fu GH, Hussain Y (2023) New insights into the anomaly genesis of the frequency selection method: supported by numerical modeling and case studies. Pure Appl Geophys 180:969–982. https://doi.org/10.1007/s00024-022-03220-8
12. Song W, Li Z, Jin Y, Zhang B, Zheng T (2021) Comprehensive application of hydrogeological survey and in-situ thermal response test. Case Stud Therm Eng 27:101287. https://doi.org/10.1016/j.csite.2021.101287
13. Alabi AA, Popoola OI, Olurin OT, Ogungbe AS, Ogunkoya OA, Okediji SO (2020) Assessment of groundwater potential and

quality using geophysical and physicochemical methods in the basement terrain of southwestern. Niger Environ Earth Sci 79:364. https://doi.org/10.1007/s12665-020-09107-y

14. Bayowa OG, Adagunodo TA, Akinluyi FO, Hamzat WA (2023) Geo-electrical exploration of the Coastal Plain Sands of Okitipupa area, southwestern Nigeria. Int J Environ Sci Technol 20:6365–6382. https://doi.org/10.1007/s13762-022-04393-4

15. Adagunodo TA, Akinloye MK, Sunmonu LA, Aizebeokhai AP, Oyeyemi KD, Abodunrin FO (2018) Groundwater exploration in Aaba residential area of Akure. Niger Front Earth Sci 6:66. https://doi.org/10.3389/feart.2018.00066

16. SDG (Sustainable Development Goals) (2019) The human rights guide to the sustainable development goals: goals, targets and indicators. The Danish Institute for Human Rights, Wilders Plads 8K, 1403 Copenhagen K, Denmark. https://sdg.humanrights.dk/en/goals-and-targets. Accessed 30 Nov 2022

17. Adagunodo TA, Aremu AA, Bayowa OG, Ojoawo AI, Adewoye AO, Olonade TE (2023) Assessment and health effects of radon and its relation with some parameters in groundwater sources from shallow granitic terrains, southeastern axis of Ibadan. Niger Groundw Sustain Dev 21:100930. https://doi.org/10.1016/j.gsd.2023.100930

18. Oladapo OO, Adagunodo TA, Aremu AA, Oni OM, Adewoye AO (2022) Evaluation of soil-gas radon concentrations from different geological units with varying strata in a crystalline basement complex of southwestern Nigeria. Environ Monit Assess 194:486. https://doi.org/10.1007/s10661-022-10173-x

19. Coker JO, Rafiu AA, Abdulsalam NN, Ogungbe AS, Olajide AA, Agbelemoge AJ (2021) Investigation of groundwater contamination from Akanran open waste dumpsite, Ibadan, south-western Nigeria, using geoelectrical and geochemical techniques. J Niger Soc Phys Sci 3:89–95. https://doi.org/10.46481/jnsps.2021.166

20. Oladejo OP, Adagunodo TA, Sunmonu LA, Adabanija MA, Enemuwe CA, Isibor PO (2020) Aeromagnetic mapping of fault architecture along lagos-ore axis, Southwestern Nigeria. Open Geosci 12:376–389. https://doi.org/10.1515/geo-2020-0100

21. Alao JO, Yusuf MA, Nur MS, Nuruddeen AM, Ahmad MS, Jaiyeoba E (2023) Delineation of aquifer promising zones and protective capacity for regional groundwater development and sustainability. SN Appl Sci 5:149. https://doi.org/10.1007/s42452-023-05371-2

22. Joel ES, Olasehinde PI, Adagunodo TA, Omeje M, Oha I, Akinyemi ML, Olawole OC (2020) Geo-investigation on groundwater control in some parts of Ogun state using data from shuttle radar topography mission and vertical electrical soundings. Heliyon 6(1):e03327. https://doi.org/10.1016/j.heliyon.2020.e03327

23. Adagunodo TA, Sunmonu LA (2012) Geoelectric assessment of groundwater prospect and vulnerability of overburden aquifers at Adumasun area, Oniye, Southwestern Nigeria. Arch Appl Sci Res 4(5):2077–2093

24. Obiora DN, Ibuot JC, George NJ (2016) Evaluation of aquifer potential, geoelectric and hydraulic parameters in Ezza North, southeastern Nigeria, using geoelectric sounding. Int J Environ Sci Technol 13:435–444

25. Daniel AN, Ekeleme IK, Onuigbo CM, Ikpeazu VO, Obiekezie SO (2021) Review on effect of dumpsite leachate to the environmental and public health implication. GSC Adv Res Rev 7(02):051–060

26. Ajibade OM, Ariyo SO, Oladipupo SD, Okeleye AO (2022) Geology and correlative analysis of borehole logs with geo-electric sections of some parts of Ibadan, southwestern Nigeria. Iraqi J Sci 63(8):3432–3446. https://doi.org/10.24996/ijs.2022.63.8.19

27. Popoola OI, Adenuga OA (2019) Determination of leachate curtailment capacity of selected dumpsites in Ogun state southwestern Nigeria using integrated geophysical methods. Sci Afr 6:e00208. https://doi.org/10.1016/j.sciaf.2019.e00208

28. Aharoni I, Siebner H, Dahan O (2017) Application of vadose-zone monitoring system for real-time characterization of leachate

percolation in and under a municipal landfill. Waste Manage 67:201–213

29. Adagunodo TA, Sunmonu LA, Oladejo OP, Olafisoye ER (2013) Groundmagnetic investigation into the cause of the subsidence in the abandoned local government secretariat, Ogbomoso, Nigeria. ARPN J Earth Sci 2(3):101–109

30. Olawuyi AK, Abolarin SB (2013) Evaluation of vertical electrical sounding method for groundwater development in basement complex terrain of West-Central Nigeria. Niger J Technol Dev 10(2):22–28

31. Ravn NR, Michelsen A, Reboleira ASPS (2020) Decomposition of organic matter in caves. Front Ecol Evol 8:554651

32. Stegen JC, Fredrickson JK, Wilkins MJ, Konopka AE, Nelson WC, Arntzen EV, Chrisler WB, Chu RK, Danczak RE, Fansler SJ, Kennedy DW, Resch CT, Tfaily M (2016) Groundwater-Surface water mixing shifts ecological assembly processes and stimulates organic carbon turnover. Nat Commun 7:11237

33. Aharoni I, Siebner H, Yogev U, Dahan O (2020) Holistic approach for evaluation of landfill pollution potential from the waste to the aquifer. Sci Total Environ 741:140367

34. Han Z, Ma H, Shi G, He L, Wei L, Shi Q (2016) A review of groundwater contamination near municipal solid waste landfill sites in China. Sci Total Environ 569–570:1255–1264

35. Adagunodo TA, Sunmonu LA, Oladejo OP, Olanrewaju AM (2019) Characterization of soil stability to withstand erection of highrise structure using electrical resistivity tomography. In: Kallel A et al (eds) Recent advances in geo-environmental engineering, geomechanics and geotechnics, and geohazards advances in science, technology and innovation (IEREK Interdisciplinary Series for Sustainable Development). Springer, Cham

36. Aizebeokhai AP, Ogungbade O, Oyeyemi KD (2021) Application of geoelectrical resistivity for delineating crystalline basement aquifers in Basiri, Ado-Ekiti, Southwestern Nigeria. Arab J Geosci 14:51

37. Helene LPI, Moreira CA, Bovi RC (2020) Identification of leachate infiltration and its flow pathway in landfill by means of electrical resistivity tomography (ERT). Environ Monit Assess 192:249. https://doi.org/10.1007/s10661-020-8206-5

38. Sunmonu LA, Adagunodo TA, Olafisoye ER, Oladejo OP (2012) The groundwater potential evaluation at industrial estate Ogbomoso Southwestern Nigeria. RMZ-Mater Geoenviron 59(4):363–390

39. Bayewu OO, Oloruntola MO, Mosuro GO, Laniyan TA, Ariyo SO, Fatoba JO (2018) Assessment of groundwater prospect and aquifer protective capacity using resistivity method in Olabisi Onabanjo University campus, Ago-Iwoye, southwestern Nigeria. NRIAG J Astron Geophys 7:347–360

40. Mohammed MAA, Szabo NP, Szucs P (2023) Exploring hydrogeological parameters by integration of geophysical and hydrogeological methods in northern Khartoum state, Sudan. Groundw Sustain Dev 20:100891

41. Krasny J (1993) Classification of transmissivity magnitude and variation. Ground Water 31(2):230–236

42. Condon LE, Maxwell RM (2015) Evaluating the relationship between topography and groundwater using outputs from a continental-scale integrated hydrology model. Water Resour Res 51:6602–6621. https://doi.org/10.1002/2014WR016774

43. Joel ES, Olasehinde PI, Adagunodo TA, Omeje M, Akinyemi ML, Ojo JS (2019) Integration of aeromagnetic and electrical resistivity imaging for groundwater potential assessment of coastal plain sands area of Ado-Odo/Ota in Southwest Nigeria. Groundw Sustain Dev 9:100264. https://doi.org/10.1016/j.gsd.2019.100264